Natural Convection Flow and Heat Transfer Between a Fluid Layer and a Porous Layer Inside a Rectangular Enclosure

C. Beckermann

S. Ramadhyani

R. Viskanta

Heat Transfer Laboratory,
School of Mechanical Engineering,
Purdue University,
West Lafayette, IN 47907

A numerical and experimental study is performed to analyze the steady-state natural convection fluid flow and heat transfer in a vertical rectangular enclosure that is partially filled with a vertical layer of a fluid-saturated porous medium. The flow in the porous layer is modeled utilizing the Brinkman–Forchheimer–extended Darcy equations. The numerical model is verified by conducting a number of experiments, with spherical glass beads as the porous medium and water and glycerin as the fluids, in rectangular test cells. The agreement between the flow visualization results and temperature measurements and the numerical model is, in general, good. It is found that the amount of fluid penetrating from the fluid region into the porous layer depends strongly on the Darcy (Da) and Rayleigh (Ra) numbers. For a relatively low product of $Ra \times Da$, the flow takes place primarily in the fluid layer, and heat transfer in the porous layer is by conduction only. On other hand, fluid penetrating into a relatively highly permeable porous layer has a significant impact on the natural convection flow patterns in the entire enclosure.

1 Introduction

Interest in natural convection fluid flow and heat transfer in porous media has been motivated by a broad range of applications, including geothermal systems, crude oil production, storage of nuclear waste materials, ground water pollution, fiber and granular insulations, solidification of castings, etc. A comprehensive review of the literature is available (Cheng, 1978). In a wide variety of such problems, the physical system can be modeled as a two-dimensional, rectangular enclosure filled with a homogeneous porous medium, with the vertical walls held at different temperatures and the connecting horizontal walls considered adiabatic. In the past two decades, numerous experimental and theoretical investigations have been devoted to the steady-state natural convection flow and heat transfer in such enclosures. In many real situations, however, the porous medium consists of several layers of different permeability. In addition, the enclosure might contain simultaneously a (free) fluid and a porous layer. A typical example of this is a situation where porous insulation material occupies only a small fraction of the space between two walls. The fluid flow and heat transfer can be significantly reduced because of the large frictional resistance offered by the porous insulation.

The present study is motivated by natural convection in a solidifying casting. Because of the extended freezing temperature range of an alloy, a mushy zone might exist, consisting of a fine meshwork of dendrites growing into the melt region. In the past, fluid flow in this mushy zone has been modeled as natural convection in a porous medium (Fisher, 1981). There has been some controversy on the importance of fluid flow between the pure melt region and the porous mushy zone. Most investigators have neglected this phenomenon in their analyses. However, penetration of fluid into the mushy zone can significantly alter the local temperatures and concentrations in the mushy zone and, eventually, the chemical homogeneity and grain structure of the solidified casting. Hence, the objective of the present study is to investigate the natural convection flow and heat transfer in such a system, idealized as a vertical rectangular enclosure partially filled with a vertical porous layer.

Research devoted to natural convection in layered porous media is relatively new. A recent review of the subject has been provided by Tien and Hong (1985). Sun (1973), Nield (1977), and Somerton and Catton (1982) have studied convective instabilities in the case where a horizontal fluid is superposed above a porous layer, but no study has been found in the open literature concerning the vertical case considered here. Of related interest is the numerical investigation of Poulikakos and Bejan (1983) who have considered a vertical rectangular enclosure with vertical layers of various permeability porous media. Tong and Subramanian (1983) and Lauriat and Mesguich (1984) have investigated natural convection in vertical rectangular enclosures that are vertically divided into a fluid and a porous layer, the two being separated by an impermeable wall.

In the present study, fluid flow is permitted to take place between the fluid and porous layers (i.e., the partition is permeable). The flow is modeled by utilizing the Brinkman–Forchheimer–extended Darcy equations for the porous layer. The predictions of the model are verified by conducting experiments in rectangular test cells using flow visualization and temperature measurements. The heat transfer and fluid flow phenomena in the present physical system are further investigated through a number of numerical experiments. However, in view of the large number of governing parameters, no attempt has been made to present a complete parametric study.

2 Analysis

2.1 Model Equations. The physical situation and coordinate system are shown in Fig. 1. The horizontal extent of the fluid layer is s, while the overall dimensions of the rectangular enclosure are H and L. It is assumed that the flow is steady, laminar, incompressible, and two-dimensional. The thermophysical properties of the fluid are assumed constant, except for the density in the buoyancy term in the momentum

Contributed by the Heat Transfer Division and presented at the 4th AIAA/ASME Thermophysics and Heat Transfer Conference, Boston, Massachusetts, June 1–4, 1986. Manuscript received by the Heat Transfer Division March 14, 1986.

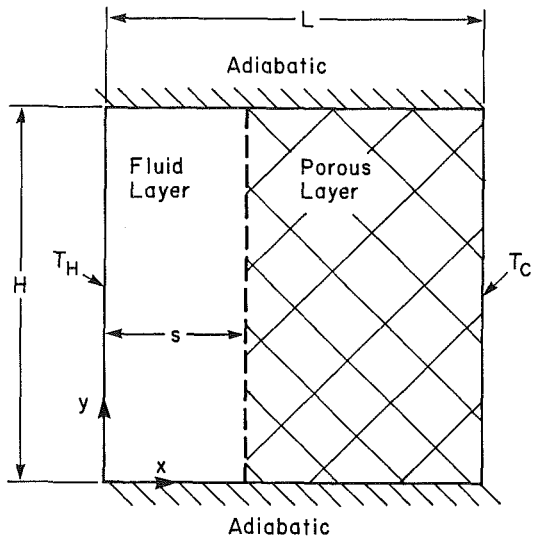

Fig. 1 Schematic of the physical model and coordinate system

equations. The porous medium is considered homogeneous and isotropic and is saturated with a fluid which is in local thermodynamic equilibrium with the solid matrix. The governing conservation equations for the fluid and the porous layer will be written separately. For the fluid layer, we have:

Continuity:

$$\frac{\partial U}{\partial x}+\frac{\partial V}{\partial y}=0 \tag{1}$$

Momentum:

$$\rho\left(U\frac{\partial U}{\partial x}+V\frac{\partial U}{\partial y}\right)=-\frac{\partial P}{\partial x}+\frac{\partial}{\partial x}\left(\mu_f\frac{\partial U}{\partial x}\right)+\frac{\partial}{\partial y}\left(\mu_f\frac{\partial U}{\partial y}\right) \tag{2}$$

$$\rho\left(U\frac{\partial U}{\partial x}+V\frac{\partial U}{\partial y}\right)=-\frac{\partial P}{\partial y}+\frac{\partial}{\partial x}\left(\mu_f\frac{\partial V}{\partial x}\right)+\frac{\partial}{\partial y}\left(\mu_f\frac{\partial V}{\partial y}\right)+\rho g\beta(T-T_c) \tag{3}$$

Energy:

$$\rho c_{pf}\left(U\frac{\partial T}{\partial x}+V\frac{\partial T}{\partial y}\right)=\frac{\partial}{\partial x}\left(k_f\frac{\partial T}{\partial x}\right)+\frac{\partial}{\partial y}\left(k_f\frac{\partial T}{\partial y}\right) \tag{4}$$

The conservation equations for the porous layer are based on a non-Darcian model, incorporating the Brinkman and Forchheimer extensions to account for viscous and inertia effects, respectively. The importance of these extensions is discussed in Beckermann et al. (1986a and 1987), who have found that both extensions must be included simultaneously for a high permeability porous medium (i.e., a high Darcy number), while the importance of Forchheimer's extension increases with decreasing Pr/R_k. In terms of the superficial (Darcian) velocity, the governing equations for the porous layer are (Tien and Hong, 1985; Georgiadis and Catton, 1984):

Continuity:

$$\frac{\partial U_D}{\partial x}+\frac{\partial V_D}{\partial y}=0 \tag{5}$$

Momentum:

$$0=-\frac{\partial P}{\partial x}+\frac{\partial}{\partial x}\left(\mu_{\text{eff}}\frac{\partial U_D}{\partial x}\right)+\frac{\partial}{\partial y}\left(\mu_{\text{eff}}\frac{\partial U_D}{\partial y}\right)-\left(\frac{\mu_f}{K}+\frac{\rho C}{\sqrt{K}}\,|\mathbf{U}_D|\right)U_D \tag{6}$$

$$0=-\frac{\partial P}{\partial y}+\frac{\partial}{\partial x}\left(\mu_{\text{eff}}\frac{\partial V_D}{\partial x}\right)+\frac{\partial}{\partial y}\left(\mu_{\text{eff}}\frac{\partial V_D}{\partial y}\right)+\rho g\beta(T-T_c)-\left(\frac{\mu_f}{K}+\frac{\rho C}{\sqrt{K}}\,|\mathbf{U}_D|\right)V_D \tag{7}$$

Energy:

$$\rho c_{pf}\left(U_D\frac{\partial T}{\partial x}+V_D\frac{\partial T}{\partial y}\right)=\frac{\partial}{\partial x}\left(k_{\text{eff}}\frac{\partial T}{\partial x}\right)+\frac{\partial}{\partial y}\left(k_{\text{eff}}\frac{\partial T}{\partial y}\right) \tag{8}$$

The boundary conditions for the governing equations for both the fluid and the porous layer are the no-slip condition at the impermeable walls of the enclosure as well as the constant temperature and zero heat flux conditions at the vertical and horizontal walls, respectively. The two sets of equations are coupled by the following matching conditions at the porous/fluid layer interface

$$T|_{x=s^-}=T|_{x=s^+} \tag{9a}$$

$$k_f\frac{\partial T}{\partial x}\Big|_{x=s^-}=k_{\text{eff}}\frac{\partial T}{\partial x}\Big|_{x=s^+} \tag{9b}$$

$$U|_{x=s^-}=U_D|_{x=s^+},\quad V|_{x=s^-}=V_D|_{x=s^+} \tag{9c}$$

Nomenclature

A = aspect ratio = H/L
c_p = specific heat, J/kg K
C = inertial coefficient, see equation (11)
Da = Darcy number = K/L^2
g = gravitational acceleration, m/s^2
$\bar{h}$ = average convective heat transfer coefficient, W/m^{2}K
H = height of enclosure, m
k = thermal conductivity, W/mK
K = permeability of the porous medium, m^2
L = length of enclosure, m
$\overline{\mathrm{Nu}}$ = average Nusselt number = $\bar{h}L/k_f$
P = pressure, Pa
p = dimensionless pressure = $PL^2/(\rho\alpha_f^2)$
Pr = Prandtl number = ν_f/α_f
Ra = Rayleigh number = $g\beta(T_H-T_C)L^3/(\nu_f\alpha_f)$
R_k = ratio of thermal conductivities = k_{eff}/k_f
s = fluid layer thickness, m
S = dimensionless fluid layer thickness = s/L
T = temperature, K
u = dimensionless x-component velocity = UL/α_f
U = x-component velocity, m/s
v = dimensionless y-component velocities = VL/α_f
V = y-component velocity, m/s
x = horizontal coordinate, m
X_p = binary parameter, see equation (13)
y = vertical coordinate, m
α = thermal diffusivity = $k_f/\rho c_{pf}$, m^2/s
β = coefficient of thermal expansion, K^{-1}
ϵ = porosity of the porous medium
η = dimensionless vertical coordinate = y/L
θ = dimensionless temperature = $(T-T_C)/(T_H-T_C)$
μ = dynamic viscosity, Ns/m^2
ν = kinematic viscosity, m^2/s
ξ = dimensionless horizontal coordinate = x/L
ρ = fluid density, kg/m^3

Subscripts

b = beads
C = cold
D = Darcy
eff = effective
f = fluid
H = hot

$$P|_{x=s^-} = P|_{x=s^+} \tag{9d}$$

$$\mu \frac{\partial U}{\partial x}\Big|_{x=s^-} = \mu_{\text{eff}} \frac{\partial U_D}{\partial x}\Big|_{x=s^+} \tag{9e}$$

$$\mu\left(\frac{\partial V}{\partial x}+\frac{\partial U}{\partial y}\right)\Big|_{x=s^-} = \mu_{\text{eff}}\left(\frac{\partial V_D}{\partial x}+\frac{\partial U_D}{\partial y}\right)\Big|_{x=s^+} \tag{9f}$$

Equations (9*a*), (9*b*), (9*c*), and (9*d*) express the continuity of temperature, heat flux, normal and tangential velocities, and pressure, respectively, across the fluid/porous layer interface. Equations (9*e*) and (9*f*) are the matching conditions for the deviative normal and shear stresses. Note that equations (9*d*) and (9*e*) taken together imply matching of the total normal stress at the interface. Equation (9*f*) represents an extension of the shear stress matching condition of Neale and Nader (1974) for flow which is not parallel to the fluid/porous layer interface. Obviously, matching of the stresses at the interface can only be accomplished if Brinkman's extension is used in the momentum equations for the porous layer.

The values for the permeability K and the inertia coefficient C in the momentum equations for the porous layer are given by Ergun (1952) for packed beds of beads of diameter d_b and porosity ϵ

$$K = \frac{d_b^2 \epsilon^3}{175(1-\epsilon)^2} \tag{10}$$

$$C = \frac{1.75}{\sqrt{175}}\,\epsilon^{-3/2} \tag{11}$$

In addition, models for the effective properties (μ_{eff} and k_{eff}) of the porous medium are needed. It has been found that taking $\mu_{\text{eff}} = \mu_f$ in Brinkman's extension provides good agreement with experimental data (Neale and Nader, 1974; Lundgren, 1972) and is adopted in the present work. Various models for the effective thermal conductivity k_{eff} have been proposed (Combarnous and Bories, 1975). In the present study, a nonlinear equation derived by Veinberg (1967) is used, which is claimed to be universally applicable for a medium with randomly distributed spherical inclusions

$$k_{\text{eff}} + \epsilon\left(\frac{k_b - k_f}{k_f^{1/3}}\right)k_{\text{eff}}^{1/3} - k_b = 0 \tag{12}$$

2.2 Dimensionless Equations. Instead of solving the governing equations separately for each layer, the equations are combined into one set by introducing the following binary parameter

$$X_p(\xi,\eta) = \begin{cases} 1 & \text{if in porous layer } 0<\epsilon<1 \\ 0 & \text{if in fluid layer } \epsilon = 1 \end{cases} \tag{13}$$

Introducing dimensionless variables (see the Nomenclature), the combined conservation equations for the fluid and porous layer can be written as:

Continuity:

$$\frac{\partial u}{\partial \xi}+\frac{\partial v}{\partial \eta} = 0 \tag{14}$$

Momentum:

$$(1-X_p)\left(u\frac{\partial u}{\partial \xi}+v\frac{\partial u}{\partial \eta}\right) = -\frac{\partial p}{\partial \xi}+\text{Pr}\left(\frac{\partial^2 u}{\partial \xi^2}+\frac{\partial^2 u}{\partial \eta^2}\right)-X_p\left(\frac{\text{Pr}}{\text{Da}}+\frac{C}{\sqrt{\text{Da}}}|\mathbf{u}|\right)u \tag{15}$$

$$(1-X_p)\left(u\frac{\partial v}{\partial \xi}+v\frac{\partial v}{\partial \eta}\right) = -\frac{\partial p}{\partial \eta}+\text{Pr}\left(\frac{\partial^2 v}{\partial \xi^2}+\frac{\partial^2 v}{\partial \eta^2}\right)-X_p\left(\frac{\text{Pr}}{\text{Da}}+\frac{C}{\sqrt{\text{Da}}}|\mathbf{u}|\right)v+\text{RaPr}\theta \tag{16}$$

Energy:

$$u\frac{\partial \theta}{\partial \xi}+v\frac{\partial \theta}{\partial \eta} = (X_p(R_k-1)+1)\left(\frac{\partial^2 \theta}{\partial \xi^2}+\frac{\partial^2 \theta}{\partial \eta^2}\right) \tag{17}$$

By combining the governing equations for the two regions, the fluid and the porous media are treated as a single medium with its properties depending on the location within the enclosure. The advantage of this formulation is that it ensures the satisfaction of the matching conditions at the fluid/porous layer interface and, thus, simplifies the numerical solution procedure (refer to the following section). It is interesting to consider the limiting case when the porous medium has a high porosity, because this situation should closely approximate natural convection in a purely fluid enclosure. In this limit, as $\text{Da} \to \infty$ and $R_k \to 1$, the governing equations on the porous side begin to resemble the fluid side equations. Indeed, the principal difference between the porous and fluid side equations is the absence of inertia terms in the momentum equations for the porous side. At moderate Rayleigh numbers, since inertia effects are small, the present formulation is able to reproduce the velocity and temperature distributions corresponding to a purely fluid enclosure when Da is assigned a very large value (Beckermann et al., 1986a). The boundary conditions for the combined equations are given in dimensionless form as

$$\begin{aligned} &\theta = 1, \quad u = v = 0 \text{ at } \xi = 0, \quad 0 \le \eta \le A \\ &\theta = 0, \quad u = v = 0 \text{ at } \xi = 1, \quad 0 \le \eta \le A \\ &\frac{\partial \theta}{\partial \eta} = 0, \quad u = v = 0 \text{ at } \eta = 0, \quad 0 \le \xi \le 1 \\ &\frac{\partial \theta}{\partial y} = 0, \quad u = v = 0 \text{ at } \eta = A, \quad 0 \le \xi \le 1 \end{aligned} \tag{18}$$

The results for the total heat transfer rate across the enclosure will be presented in terms of the Nusselt number defined as

$$\overline{\text{Nu}} = \frac{\bar{h}L}{k_f} = -\frac{1}{A}\int_0^A (X_p(R_k-1)+1)\frac{\partial \theta}{\partial \xi}\Big|_{\substack{\xi=1 \\ \text{or} \\ \xi=0}} d\eta \tag{19}$$

According to this definition, the actual heat transfer rate is referenced to the heat transfer by conduction if the entire enclosure is filled with the fluid alone.

2.3 Numerical Procedure. The combined continuity, momentum, and energy equations (14)–(17) were solved numerically using the SIMPLER algorithm (Patankar, 1980). The control-volume formulation utilized in this algorithm ensures continuity of the convective and diffusive fluxes as well as overall momentum and energy conservation. The harmonic mean formulation adopted for the interface diffusion coefficients between two control volumes can handle abrupt changes in these coefficients (for example, if $R_k \neq 1$) without requiring an excessively fine grid, for example, at the porous/fluid layer interface.

The mesh size required for sufficient numerical accuracy depended mainly on the Rayleigh and Darcy numbers. For most of the numerical experiments, a grid of 25×25 nodal points ensured independence of the solution on the grid. The nodal points were uniformly distributed in the y direction, while the distribution along the x direction was slightly skewed to have a greater concentration of points near the vertical

Table 1 Summary of experimental conditions ($A = 1.0, S = 0.5$)

Test No.	Test cell/ fluid	d_b [mm]	Ra	Pr	Da	C	R_k	Ra•Da
1	small t.c./water	1.6	3.028×10^{7}	6.97	7.354×10^{-7}	0.6124	1.397	22.3
2	small t.c./water	6.0	3.028×10^{7}	6.97	1.296×10^{-5}	0.5647	1.383	392.4
3	large t.c./glycerin	1.6	3.471×10^{6}	12630	3.985×10^{-8}	0.6124	2.315	0.14
4	large t.c./glycerin	6.0	3.471×10^{6}	12630	7.112×10^{-7}	0.5647	2.259	2.47

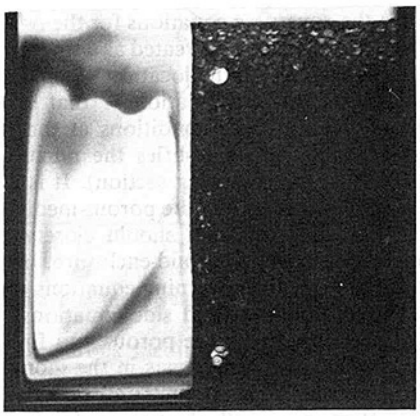

Fig. 2(a) Flow visualization

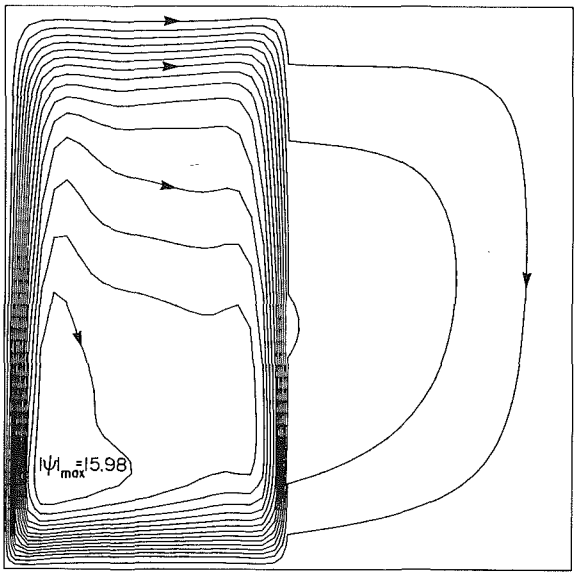

Fig. 2(b) Streamlines (equal increments)

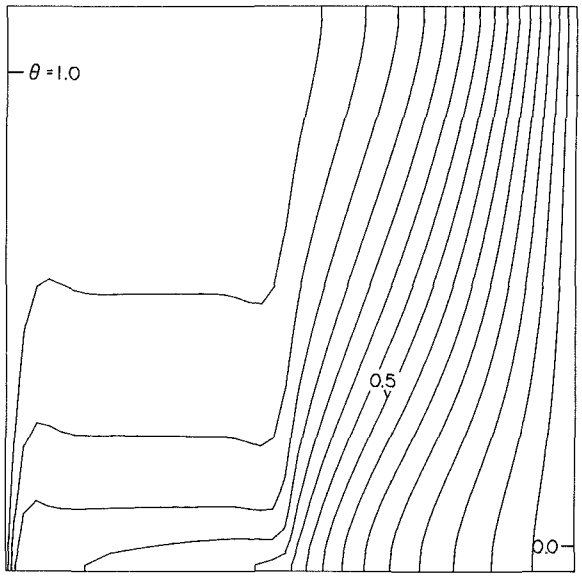

Fig. 2(c) Isotherms (equal increments)

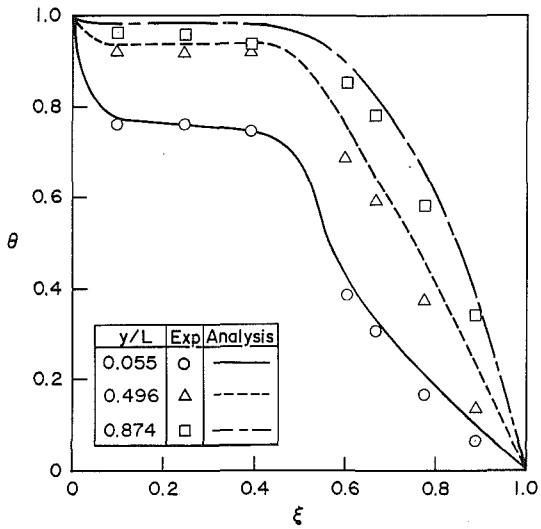

Fig. 2(d) Temperature profiles

Fig. 2 Experimental and predicted results for experiment 1 (water/small glass beads)

boundaries. For the comparisons with the experimental results (refer to Section 4), a grid of 50×50 nodal points was used. The iteration procedure was terminated when the dependent variables agreed to four significant digits. Convergence of the numerical solution was also checked by comparing the Nusselt numbers obtained along the two vertical side walls, equation (19). The agreement between the two values was always better than 0.1 percent. The calculations were performed on a CYBER 205 computer and required between 50 and 500 CPU seconds (depending on the mesh size and the Rayleigh and Darcy numbers). A test of the accuracy of the numerical algorithm was obtained by comparing the results to those reported in the literature for the limiting cases of a fully porous and a fully fluid enclosure. The results of these comparisons are given by Beckermann et al. (1986a).

3 Experiments

3.1 Test Cell and Instrumentation. Natural convection experiments were performed in two different test cells of square cross section partially filled with a porous medium. The smaller test cell had inside dimensions of 4.76 cm in height and width and 3.81 cm in depth, while the larger test cell measured 20.32 cm in height and width and 3.0 cm in depth. In both test cells, the two vertical sidewalls, which served as the heat source/sink, were multipass counterflow heat exchangers machined out of a copper plate. For flow visualization purposes, the vertical front and back walls were made of plexiglass. The horizontal top and bottom walls were made of acrylic and phenolic plates, respectively. The test cells were insulated with 5.09-cm-thick Styrofoam.

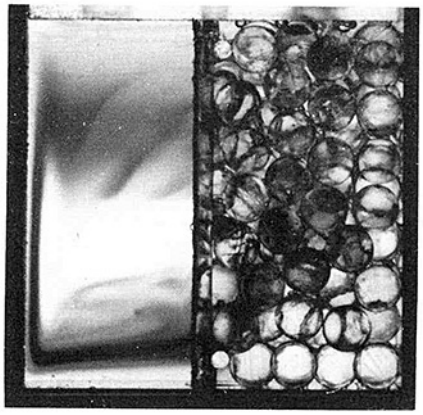

Fig. 3(*a*) Flow visualization

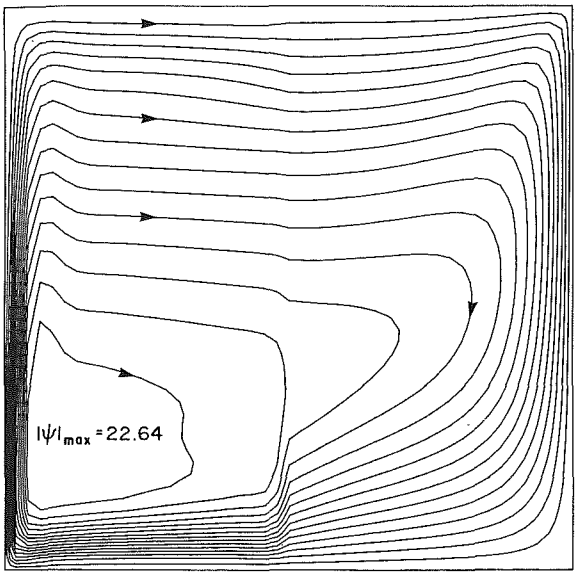

Fig. 3(*b*) Streamlines (equal increments)

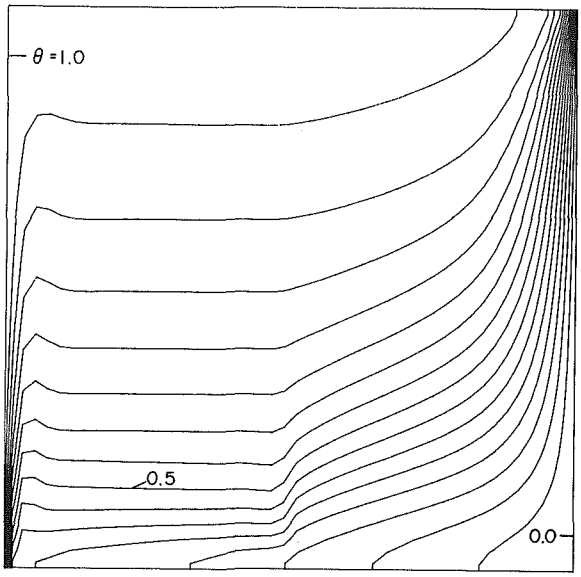

Fig. 3(*c*) Isotherms (equal increments)

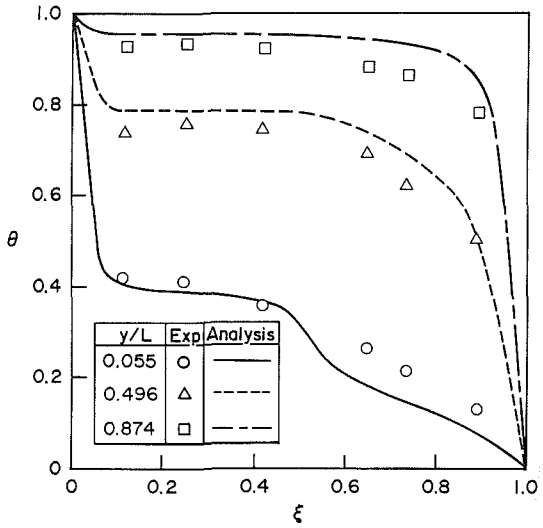

Fig. 3(*d*) Temperature profiles

Fig. 3 Experimental and predicted results for experiment 2 (water/large glass beads)

The temperatures of the copper heat exchangers were measured with five thermocouples epoxied separately into five small-diameter holes which were drilled close to the surface of the copper plates. The temperature distribution in the smaller test cell was measured using a movable thermocouple probe sheathed in a 1.27 mm o.d. stainless steel tube. The position of the thermocouple bead in the test cell was determined with a slide caliper. It was estimated that the position of the bead could be determined to within ± 0.5 mm. It should also be noted that the structure of the porous medium was slightly disturbed due to the movement of the thermocouple probe especially in the case of the large glass beads. This disturbance, however, is believed to have had a relatively small influence on the temperature measurements. After each movement of the thermocouple probe, the system was allowed to reach steady state again.

Measurement of the temperature distribution in the larger test cell was made with 28 thermocouples with a wire diameter of 0.127 mm which were placed in three different plexiglass rakes. The three rakes were located along the center line at heights of 2.86, 10.16, and 17.78 cm measured from the bottom of the test cell. All thermocouples were calibrated with an accuracy of ± 0.1°C.

3.2 Test Materials. Spherical glass beads were used as the porous medium. The beads were of soda-lime glass with diameters of 1.59 and 6.0 mm. The properties used were for a soda-lime glass with a chemical composition closely matching that of the glass beads used in this study (Weaver, 1985). The glass beads were held in place by a fine fiberglass screen supported by small diameter glass rods. The porosity of the screen was much higher than the porosity of the glass beads, while the mesh size was only slightly smaller than the diameter of the glass beads. It is believed that the screen had a negligible influence on the flow and heat transfer between the porous and fluid layers. In all experiments, the porous medium was a vertical layer occupying half of the test cell. The porosity was measured separately for each size glass bead (Weaver, 1985). For the large diameter glass beads, the increase in porosity near the walls of the test cells is more significant (considering the relatively small depth of the test cells) resulting in a higher value of the average porosity.

The fluids used were once-distilled, degasified water for the smaller test cell and chemical grade glycerin for the larger test cell. With the various combinations of fluids, glass beads, and test cells, it was possible to cover a broad range of the relevant dimensionless parameters. The values of the dimensionless parameters for the four experiments selected for comparison

with the numerical results are summarized in Table 1. All properties were evaluated at a temperature of $(T_H + T_C)/2$.

3.3 Experimental Procedures. In preparing for the experiment, one half of the test cell was first filled with the glass beads. Then, the water/glycerin was carefully siphoned into the test cell to ensure that no air was trapped in the matrix or to prevent air from mixing with the fluid. A mixture of alcohol and water was circulated through the two heat exchangers from two constant temperature baths. After the system reached steady state (after at least 12 hr), the thermocouple output was read using a data logger.

Flow visualization experiments were performed in the small test cell by injecting a Calcoid Blue ink/water solution at the top of the cold heat exchanger. The test cell was illuminated from the back through the plexiglass windows by using a white light source and a diffusing white glass plate. The dye was allowed to convect with the flow for some time and the entire test cell was then photographed from the front. No flow visualization was performed in the larger test cell with glycerin as the fluid.

4 Results and Discussion

4.1 Comparison of Predictions With Experiments. With the two different glass bead sizes used in the experiments in the smaller test cell, it was possible to cover a relatively broad range of Darcy numbers (from about 7.4×10^{-7} to 1.3×10^{-5}), while the other dimensionless parameters were approximately constant. The results of these experiments, together with the pertinent numerical predictions, are shown in Figs. 2 and 3. The values of the governing parameters corresponding to the figures are listed for the respective experiments in Table 1. It can be seen from both the flow visualization and the predicted streamlines, that with increasing permeability (i.e., Darcy number) the flow penetrates progressively more into the porous layer. In the case of the small glass beads (Fig. 2), the flow is almost completely confined to the fluid layer and is not able to penetrate into the porous layer. A boundary layer develops at the porous/fluid layer interface. On the other hand, in the case of the large glass beads (Fig. 3), the porous layer offers much less resistance to the flow and natural convection takes place in the entire cavity. For both sizes of glass bead, the streamlines show sharp changes in the slope at the fluid/porous layer interface. When the flow enters the porous matrix at the upper region of the test cell, the streamlines bend upward. Due to the strong downflow along the fluid/porous layer interface, the streamlines bend downward when the flow leaves the porous region. The above observations indicate that the porous matrix exerts a strong influence on the velocity component parallel to the interface (resulting in a high velocity gradient on the fluid side), while the normal velocity component is relatively unaffected. Both velocity components are actually continuous across the fluid/porous layer interface. Also, the center about which the flow circulates is moved toward the lower left corner of the test cell when compared to natural convection in a vertical cavity filled with a homogeneous medium.

In general, the agreement between the flow patterns revealed by the flow visualization experiments and the numerically predicted streamlines is good. With the dye injection method employed in the present study, it was not possible, however, to visualize the flow patterns in the porous layer. This is mainly due to scattering of the light by the glass beads. The sharp bending of the streamlines at the fluid/porous layer interface cannot be seen on the photographs (Figs. 2*a* and 3*a*), but it was observed during the experiments. It should also be kept in mind that, especially in

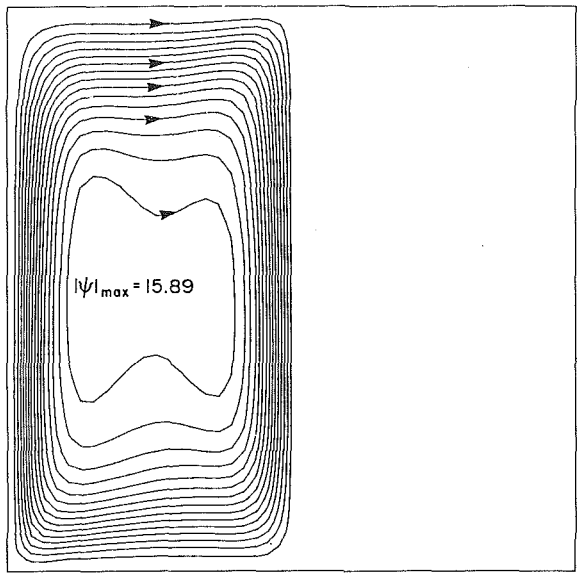

Fig. 4(*a*) Streamlines (equal increments)

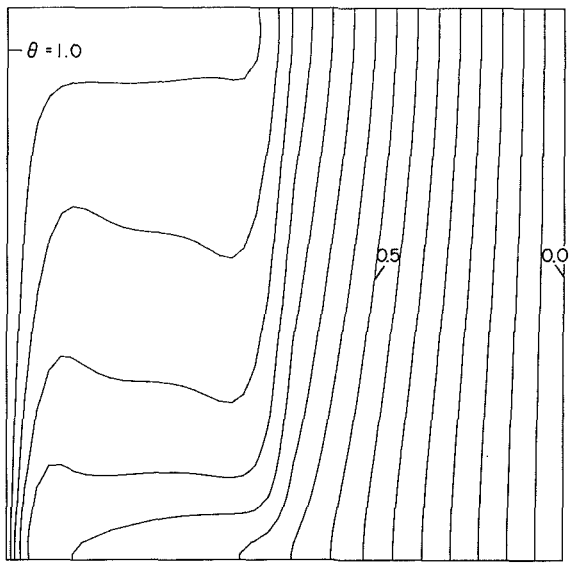

Fig. 4(*b*) Isotherms (equal increments)

Fig. 4 Numerical predictions for experiment 4 (glycerin/large glass beads)

the case of the large glass beads, there are relatively large nonuniformities in the porosity of the porous layer because of the presence of the walls. In reality, the porosity at the wall is always equal to one. This effect is, however, not taken into account in the model. It is also recognized that in experiment 2, the small size of the porous layer relative to the diameter of the glass beads might invalidate the assumptions of homogeneity and isotropy used in the derivation of the governing equations for the porous medium. The good agreement between the flow visualization and the predicted streamlines (Figs. 3*a* and 3*b*) indicates, however, that this problem is not too severe for the conditions of experiment 2.

The above observations are further supported by the predicted isotherm patterns shown in Figs. 2(*c*) and 3(*c*). In the case of the small glass beads (Fig. 2*c*) the isotherms in the porous layer are almost vertical and equally spaced, indicating that heat transfer is mainly by conduction. On the other hand, in the fluid layer, there exists a thermally stratified core in the center region with thermal boundary layers along the hot wall

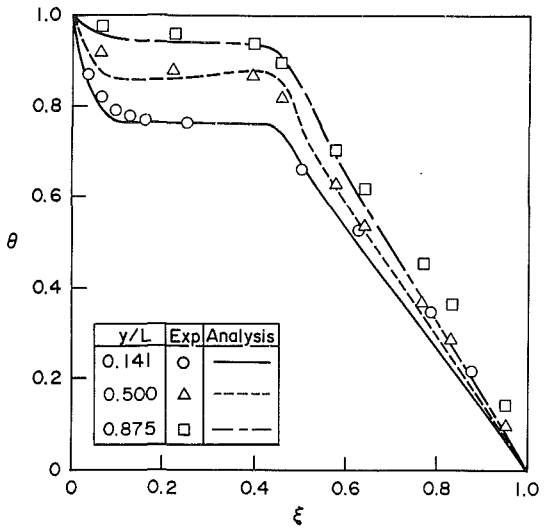

Fig. 5(*a*) Experiment 3

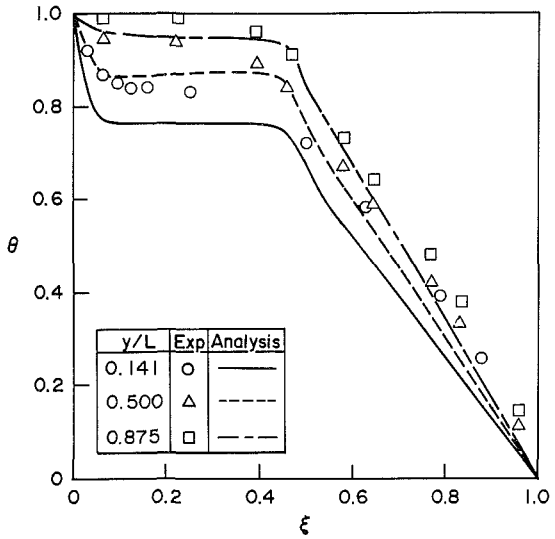

Fig. 5(*b*) Experiment 4

Fig. 5 Experimental and predicted temperature profiles (glycerin/large glass beads)

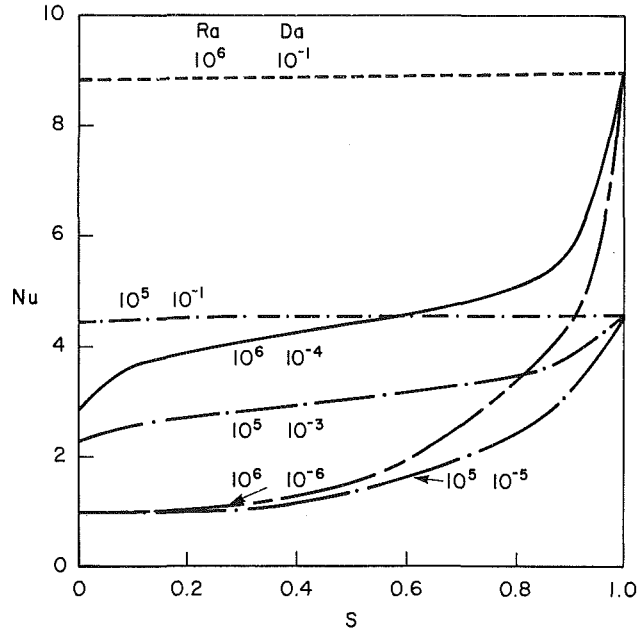

Fig. 6 Effect of fluid layer thickness on the Nusselt number (Pr = 1.0, R_k = 1.0, A = 1.0, C = 0.55)

and the porous/fluid layer interface, indicating strong natural convection flow. In the case of the large glass beads (Fig. 3*c*), the isotherms show that the fluid is thermally stratified throughout the test cell, while there are thermal boundary layers of different thickness at the hot and cold walls. In other words, the penetrating fluid causes the heat in the porous layer to be transferred convectively. In both cases, the isotherms show "cusps" at the porous/fluid layer interface which can be attributed to the natural convection flow and the difference in the thermal conductivity between the porous and fluid layers.

A quantitative comparison between measured and predicted temperatures is shown in Figs. 2(*d*) and 3(*d*). As mentioned earlier, temperature measurements were taken at three different heights in the small test cell. The general agreement between measured and predicted temperatures is good, and the differences in the temperature distributions between the experiments with the small and large glass beads are well predicted by the numerical model. It should be noted that the data trends become somewhat exaggerated due to the dimensionless representation. In reality, the discrepancies between the measured and predicted temperatures are less than about ± 1°C. A large part of these discrepancies is possibly due to the inaccuracies in determining the exact position of the movable thermocouple probe (refer to Section 3). Again, nonuniformities in the porosity at the walls are expected to produce a considerable difference between the numerical model and the experiments in the relatively small test cell of the present study.

In order to validate the model for various Rayleigh and Prandtl numbers as well as for different thermal conductivity ratios, experiments were also performed in a larger test cell with glycerin as the fluid (refer to Table 1). Although the same diameter glass beads were used in the experiments in the larger test cell, the Darcy numbers are two orders of magnitude lower than in the smaller test cell because of the larger length scale (i.e., L). Due to the high viscosity of glycerin, the Rayleigh number is one order of magnitude lower and the Prandtl number is much higher than in the experiments with water. Also, the thermal conductivity ratio is higher in the case of glycerin.

The predicted streamlines and isotherms for the case of the large glass beads (experiment 4) are illustrated in Fig. 4. (The numerical results for experiment 3 are presented in Beckermann et al. (1986a).) It can be seen that even for the large glass beads, the flow is almost completely confined to the fluid layer and very little penetration of glycerin into the porous layer takes place. Accordingly, the heat transfer in the porous layer is mainly by conduction (Fig. 4*b*). The streamlines in the fluid layer (Fig. 4*a*) show a behavior similar to what would be expected for natural convection in a vertical enclosure of the same aspect ratio as the fluid layer. In other words, even for the large glass beads the porous layer acts almost like a solid wall.

The measured and predicted temperature profiles for both sizes of glass beads (Figs. 5*a* and 5*b*) show that approximately 70 percent of the total temperature drop across the test cell takes place in the porous layer. The agreement between the slopes of the measured and predicted temperature profiles in the porous layer is very good, indicating the correctness of the model adopted for the effective thermal conductivity [equation (12)]. Also, the agreement is good for the general trend of the temperature profiles in the fluid layer. Both the measured and predicted temperature profiles show strong discontinuities in the slope at the porous/fluid layer interface which is due to the large differences in the thermal conductivities of the two

layers. The relatively large discrepancies in the absolute values of the temperatures in the case of the large glass beads (Fig. 5*b*) can be attributed to the larger nonuniformities in the porosity at the walls of the relatively thin test cell. In addition, the viscosity of glycerin varies by almost an order of magnitude over the temperature range in the present experiments (10°C). Both of the above effects are not taken into account in the model.

In summary, the comparison between measured and predicted data shown above established some confidence in the numerical model of the present study. Several "real" effects, namely, porosity and property variations, need more attention to obtain better agreement between experimental and numerical results.

4.2 Effect of Fluid Layer Thickness on the Nusselt Number. The effects of various fluid layer thicknesses S on the Nusselt number were determined numerically and are illustrated in Fig. 6. As expected, for (unrealistically) high Darcy numbers (i.e., $\mathrm{Da}=0.1$), the porous layer has nearly no effect on the heat transfer across the enclosure. The flow penetrates completely into the porous layer and natural convection is only slightly reduced. On the other hand, in the case of relatively low Darcy numbers (i.e., $\mathrm{Da}=1\times10^{-6}$ and $\mathrm{Da}=1\times10^{-5}$) the Nusselt number decreases sharply with decreasing fluid layer thickness. For these Darcy (and Rayleigh) numbers, only a small amount of fluid enters the porous layer, and the porous layer acts almost like a solid wall (see also Fig. 5). A further decrease in the Darcy number (for the same Rayleigh number) has practically no influence on the functional relationship between the Nusselt number and the fluid layer thickness. This observation is also supported by the fact that for an impermeable partition between the porous and fluid layers (Tong and Subramanian, 1983), the predicted decrease in the Nusselt number with decreasing fluid layer thickness is very similar to the decrease predicted for low Darcy numbers in the present study.

Quite different behavior can be seen for $\mathrm{Da}=1\times10^{-4}$ and $\mathrm{Da}=1\times10^{-3}$. Here, a small addition of a porous layer causes a sharp decrease in the Nusselt number. The decrease in the Nusselt number is, however, less sharp and approximately linear for further increases in the porous layer thickness and is again more pronounced when the enclosure is almost completely occupied by the porous layer (i.e., $S < 0.1$). This phenomenon can be explained by the fact that for Darcy numbers of the order of 1×10^{-4} (and a Rayleigh number of 1×10^{6}), the flow does penetrate into the porous layer. In this case, the penetrating fluid significantly alters the fluid flow in the fluid layer, i.e., the flow in the fluid layer is not similar to the natural convection patterns seen in a vertical enclosure of that aspect ratio (see also Figs. 2*a* and 3*a*). Hence, decreasing the thickness of the fluid layer has a completely different effect on the Nusselt number than in the case of low Darcy numbers where the flow is simply blocked by the porous layer.

In order to provide a quantitative criterion for the importance of penetration of fluid into the porous layer for the present physical system, many more numerical and experimental studies are needed. In particular, the effects of variations in the other dimensionless parameters, namely Pr, A, and R_k, need to be investigated. The experimental and numerical results (refer to Table 1 and Fig. 6, respectively) as well as additional numerical studies (Beckermann et al., 1986b) indicate, however, that the product $\mathrm{Ra}\times\mathrm{Da}$ should be greater than about 50 in order for penetration of fluid into the porous layer to be significant.

The coupling of the fluid flow in the porous and fluid layers is of particular importance in the solidification of castings. Here, the dendrites growing into the melt can form a highly permeable porous layer. The flow penetrating into the dendritic meshwork will not only alter the local conditions in this region but may also influence the natural convection patterns in the entire casting.

5 Conclusions

A model has been developed for natural convection in vertical enclosures containing simultaneously a fluid layer and a porous layer. The numerical results show good agreement with experiments conducted utilizing various glass beads, fluids, and test-cell sizes.

The effect of fluid layer thicknesses on the Nusselt number has been numerically investigated for various Rayleigh and Darcy numbers. It has been found that, if fluid penetrates into the porous layer, the natural convection patterns in the entire enclosure are significantly altered when compared to fully porous or fluid enclosures. The degree of penetration of fluid into the porous layer depends roughly on the product of the Rayleigh and Darcy numbers, which should be greater than about 50 in order for penetration to be significant.

Acknowledgments

The work reported in this paper was supported, in part, by the National Science Foundation under Grant No. CBT-8313573. Computer facilities were made available by Purdue University Computer Center.

References

Beckermann, C., Ramadhyani, S., and Viskanta, R., 1986a, "Natural Convection Flow and Heat Transfer Between a Fluid Layer and a Porous Layer Inside a Rectangular Enclosure," in: *Natural Convection in Porous Media*, V. Prasad and N. A. Hussein, eds., ASME, New York, pp. 1–12.

Beckermann, C., Viskanta, R., and Ramadhyani, S., 1986b, "Natural Convection in Vertical Enclosures Containing Simultaneously Fluid and Porous Layers," submitted to *Journal of Fluid Mechanics*.

Beckermann, C., Viskanta, R., and Ramadhyani, S., 1987, "A Numerical Study of Non-Darcian Natural Convection in a Vertical Enclosure Filled With a Porous Medium," *Numerical Heat Transfer* (in press).

Cheng, P., 1978, "Heat Transfer in Geothermal Systems," *Advances in Heat Transfer*, Academic Press, New York, Vol. 14, pp. 1–105.

Combarnous, M. A., and Bories, S. A., 1975, "Hydrothermal Convection in Saturated Porous Media," *Advances in Hydroscience*, Academic Press, New York, Vol. 10, pp. 231–307.

Ergun, S., 1952, "Fluid Flow Through Packed Columns," *Chemical Engineering Progress*, Vol. 48, pp. 89–94.

Fisher, K. M., 1981, "The Effects of Fluid Flow on Solidification of Industrial Castings and Ingots," *Physico Chemical Hydrodynamics*, Vol. 2, pp. 311–326.

Georgiadis, J., and Catton, I., 1984, "Prandtl Number Effect on Benard Convection in Porous Media," ASME JOURNAL OF HEAT TRANSFER, Vol. 108, pp. 284–290.

Lauriat, F., and Mesguich, F., 1984, "Natural Convection and Radiation in an Enclosure Partially Filled With a Porous Insulation," ASME Paper No. 84-WA/HT-101.

Lundgren, T. S., 1972, "Slow Flow Through Stationary Random Beds and Suspensions of Spheres," *Journal of Fluid Mechanics*, Vol. 51, pp. 1865–1874.

Neale, G., and Nader, W., 1974, "Practical Significance of Brinkman's Extension of Darcy's Law," *Canadian Journal of Chemical Engineering*, Vol. 52, pp. 475–478.

Nield, D. A., 1968, "Onset of Thermohaline Convection in a Porous Medium," *Water Resources Research*, Vol. 4, pp. 553–560.

Patankar, S., 1980, *Numerical Heat Transfer and Fluid Flow*, Hemisphere, New York.

Poulikakos, D., and Bejan, A., 1983, "Natural Convection in Vertically and Horizontally Layered Porous Media Heated From the Side," *International Journal of Heat and Mass Transfer*, Vol. 26, pp. 1805–1813.

Somerton, C. W., and Catton, I., 1982, "On the Natural Convection of Superposed Porous and Fluid Layers," ASME JOURNAL OF HEAT TRANSFER, Vol. 104, pp. 160–165.

Sun, W. J., 1973, "Convective Instability in Superposed Porous and Free Layers," Ph.D. Dissertation, University of Minnesota, Minneapolis, MN.

Tien, C. L., and Hong, J. T., 1985, "Natural Convection in Porous Media Under Non-Darcian and Non-uniform Permeability Conditions," in: *Natural Convection*, S. Kakac et al., eds., Hemisphere, Washington, DC.

Tong, T. W., and Subramanian, E., 1983, "Natural Convection in Rectangular Enclosures Partially Filled With a Porous Medium," *ASME-JSME Thermal Engineering Joint Conference*, ASME, New York, Vol. 1, pp. 331–338.

Veinberg, A. K., 1967, "Permeability, Electrical Conductivity, Dielectric Constant and Thermal Conductivity of a Medium With Spherical and Ellipsoidal Inclusions," *Soviet Physics—Doklady*, Vol. 11, pp. 593–595.

Weaver, J. A., 1985, "Solid-Liquid Phase Change Heat Transfer in Porous Media," MSME Thesis, Purdue University, West Lafayette, IN.